Science of Sintering, **48** (2016) 157-165

doi: 10.2298/SOS1602157O

UDK 549.632; 622.785

Microstructural and Electrical Properties of Cordierite-based Ceramics Obtained After Two-step Sintering Technique

Nina Obradović[1,*)], Suzana Filipović[1], Nataša Đorđević[2], Darko Kosanović[1], Vladimir Pavlović[1], Dragan Olćan[3], Antonije Đorđević[3,4], Martin Kachlik[5], Karel Maca[5]

[1]Institute of Technical Sciences of SASA, 11000 Belgrade, Serbia
[2]Institute for Technology of Nuclear and Other Raw Mineral Materials, 11000 Belgrade, Serbia
[3]School of Electrical Engineering, University of Belgrade, 11000 Belgrade, Serbia,
[4]Serbian Academy of Sciences and Arts, 11000 Belgrade, Serbia
[5]CEITEC BUT, Brno University of Technology, 61600 Brno, Czech Republic

Abstract:

Cordierite-based ceramic materials are attracting much interest for their various applications in industry, for manufacturing multilayer circuit boards, catalytic converters, filters, thermal insulation, kiln furniture, components of portable electronic devices, etc. In order to reduce production costs and modify cordierite-based materials, mechanical activation can be used. In this study, microstructural and electrical properties of mechanically activated MgO-Al_2O_3-SiO_2 system have been analyzed. The mixtures of MgO-Al_2O_3-SiO_2 powders were mechanically activated in a planetary ball mill for the time periods from 0 to 160 min. Morphological investigations have been performed on the obtained powders. The effects of activation and two-step sintering process on microstructure were investigated by scanning electron microscopy (SEM). Electrical measurements showed variations of the dielectric constant (ε_r) and loss tangent ($\tan\delta$) as a function of time of mechanical treatment.

Keywords: *Mechanical activation, Two-step sintering, Microstructure, Electrical properties, Cordierite.*

1. Introduction

Cordierite, one of the most important phases of the MgO-SiO_2-Al_2O_3 system, has low thermal expansion coefficient, excellent thermal shock resistance, low dielectric constant, high volume resistivity, high chemical durability, and relatively high refractoriness and mechanical strength. This ceramic material is widely used for honeycomb-shaped catalyst carriers in automobile exhaust systems, substrate material in integrated circuit boards, and also as refractory material, owing to its stability at high temperatures [1–3]. Cordierite ceramics can be prepared by conventional sintering methods, but it is difficult to sinter cordierite because of the narrow sintering range just below its incongruent melting point [4–6]. The preparation of a homogeneous and fine cordierite powder that can be sintered without sintering aids is considered to be highly desirable, due to the limitation factors of additives,

*) **Corresponding author**: nina.obradovic@itn.sanu.ac.rs

such as increase in thermal expansion coefficient and dielectric constant [7].

The process of mechanical activation as a pre-sintering powder preparation, in order to produce homogeneous mixtures, with uniform distribution of powder particles, to increase specific surface areas of particles, to make them more reactive and capable of new phase formation, and, finally, to decrease the sintering temperatures, is commonly used in ceramic processing [8]. Furthermore, this low-cost method has more advantages compared to other powder processing routes, such as shorter time of preparation, simplicity of method itself, and possibility of obtaining large quantities of the powder. The two-step sintering method is a promising approach to obtain dense ceramics because it suppresses grain growth in the final stage of sintering [9].

The main objective of this work is to investigate the effects of the mechanical activation and two-step sintering of cordierite-based material on microstructure and electrical properties of the final product.

2. Experimental procedure

Mixtures of MgO, Al_2O_3 and SiO_2 (all 99 % p. a, Sigma-Aldrich) were used in these experiments. Prior to the milling process, the precursor MgO powder was calcined at 700 ^oC for 2 h in order to remove $Mg(OH)_2$. The mixtures of $MgO+Al_2O_3+SiO_2$ in the 2:2:5 molar ratio were mechanically activated by grinding in a high-energy planetary ball mill (Fritsch Pulverisette 5) in ethanol. ZrO_2 vessels and balls were used with the powder-to-balls mass ratio of 1:40. The milling process was performed in air for 10, 40, 80, and 160 minutes. Non-activated (manually mixed in mortar with ethanol) and mechanically activated powder mixtures were denoted by MAS-0, MAS-10, MAS-40, MAS-80, and MAS-160, according to the milling time. After mixing and milling, the powders were dried at 120 ^oC for 2 h and sieved.

The binder-free powders were compacted using the uniaxial double action pressing process in an 8 mm diameter tool (Hydraulic press Ring, P-14, Veb Thuringer). The applied pressure was 392 MPa and an amount of 0.3 g of powders was used for each pressed sample. The compacts were placed in an alumina boat and heated in a tube furnace (Lenton Thermal Design Typ 1600). The samples were two-step sintered: non-isothermal up to 1300 ^oC (heating rate 20 ^oC/min, cooling rate 10 ^oC/min), and then dwell at 1200 ^oC for 10 h. The sintering process was performed in an air atmosphere. Samples that were subjected to the TSS process were denoted by MAS-0-S, MAS-10-S, MAS-40-S, MAS-80-S, and MAS-160-S, according to the activation time and sintering. Densities of all samples were established by the Archimedes method (EN 623-2).

The morphology of the powder mixtures obtained after milling was characterized by the scanning electron microscopy (JEOL JSM-6390 LV). The sintered samples were polished and then thermally etched at 1250 °C for 5 min. The thermally etched samples were covered by a golden layer to increase the conductivity of the surface before observing by an SEM (Philips XL30).

Measurements of the relative permittivity of the sintered samples, metallized on the top and bottom by silver, were performed using an Agilent E5061A network analyzer, in the frequency range between 1 MHz and 1 GHz. Samples were located in a custom-made coaxial chamber. The reflection coefficient of the chamber was measured by the analyzer and the relative complex permittivity of the samples was extracted using electromagnetic models.

3. Results and discussion

Detailed phase analysis of the starting powders obtained by means of XRD, is explained and discussed in our previous paper [10]. Based on those results, starting non-activated mixture is consisted of MgO, SiO_2 and Al_2O_3 peaks. After 10 minutes of activation, a new phase, $MgSiO_3$, was noticed. This phase composition remains till the end of the mechanical activation, except for Al_2O_3, which completely disappeared after 80 minutes. An intensive mechanical activation in the ball mill with ethanol led to a better homogeneity of the powder mixtures, particle size reduction, an increase in powder reactivity through the increase in the specific surface area, along with the formation of a new phase, after 10 minutes of activation. An approximation method showed that for the MgO and SiO_2 powders with prolonged mechanical activation, the crystallite size decreased down to nano-sized dimensions: 10.0 nm for MgO, and 17.2 and 47.5 nm for SiO_2. Furthermore, an increase in the dislocation density and lattice microstrain was observed. A slight increase in the crystallite size of the newly formed phase, $MgSiO_3$ (18.2–20.1 nm), indicates a process of recrystallization during an intensive mechanochemical activation.

The scanning electron micrographs for the starting mixtures are shown in Fig. 1. The micrograph of MAS-0 (Fig. 1a) indicates polygonal irregularly shaped particles. Powder particles are not connected and they are incoherent, which was expected if we have in mind the preparation of the initial non-activated mixture (only mixed, without milling). Ten minutes of the mechanical activation led to the attrition of powder particles, their homogenization, and better interconnections between them. That resulted in the increase of their specific surface area and, therefore, the increased reactivity of the samples. The agglomerates of Al_2O_3, which are clearly visible in the background of the SEM micrograph of MAS-10 (Fig. 1b), are covered by smaller particles of MgO and SiO_2. Further milling led to the additional reduction of powder particles with no clearly defined Al_2O_3 agglomerates. Prolonged mechanical activation of 80 min produced powder particles that had almost the same size as those in the previous mixture, but the presence of agglomerates was evident, as shown in Fig. 1. d. This is usual, as the introduction of high energy into the system with prolonged milling time always leads to a drastically increased reactivity of powder particles [11]. At the beginning of the milling process, the powder particles become reactive, capable of formation of new phases, and then, with additional energy transfer, practically forced to make agglomerates. Those agglomerates are a serious disadvantage during sintering. The particles within the MAS-160 powder are regularly shaped and around 0.2 μm in size (Fig. 1e). With prolonged milling times, no agglomerates were detected. The applied milling time had a great influence on the fragmentation of agglomerates. The obtained microstructure should provide a better sinterability, greater densification with no grain growth, and, finally, improved electrical properties [12, 13].

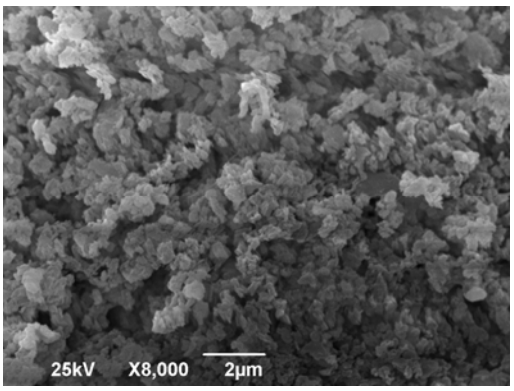

a)

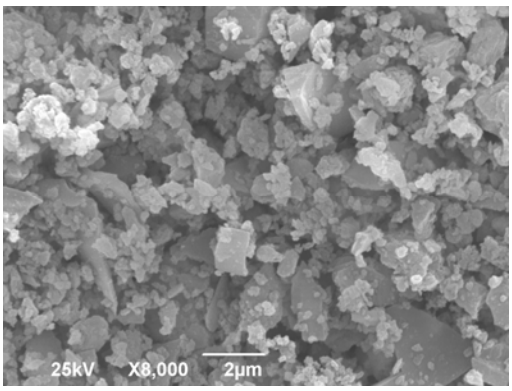

b)

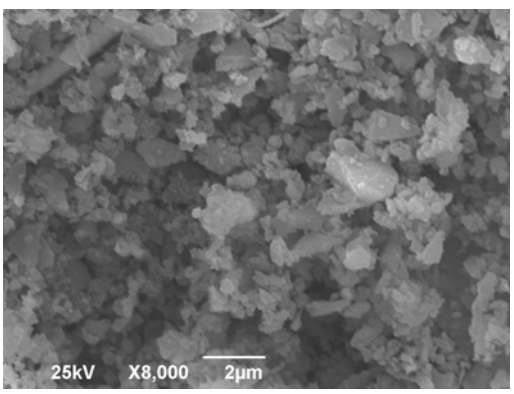

c)

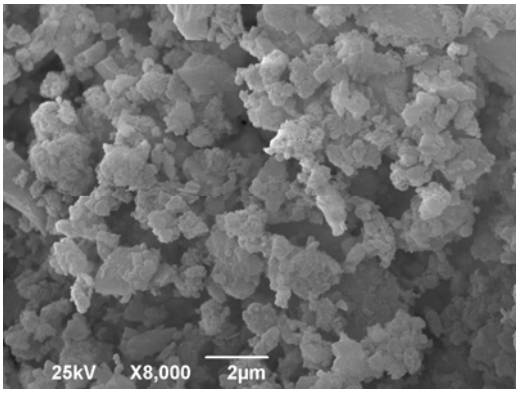

d)

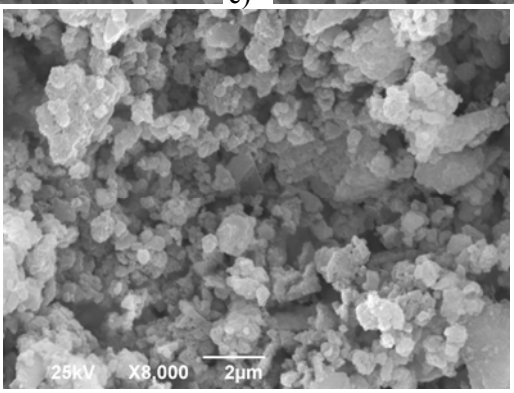

e)

Fig. 1. Scanning electron micrographs of powders: a) MAS-0, b) MAS-10, c) MAS-40, d) MAS-80, and e) MAS-160.

The scanning electron micrographs of the two-step sintered samples are shown in Fig. 2. The MAS-0-S sample (Fig. 2a) consisted of two different areas. One is a well sintered matrix and the other one is made of rod-like parts where the sintering process was not finished. This microstructure represents sintering of non-homogeneous mixture. A significant level of porosity is present in the MAS-10-S sample (Fig. 2b), higher than 31 %, and no rod-like parts are evident. Grain boundaries are well pronounced in the sample MAS-40-S (Fig. 2c), a microstructure with small grains remains, the level of densification is higher, while the open porosity is slightly decreased. The prolonged mechanical activation followed by two-step sintering did not result in significant changes in the microstructure. Grains retain their shape and size around one micron or less, decreasing the porosity negligibly, no grain growth was observed. On the other hand, the sample MAS-160-S has the highest relative density and the lowest relative open porosity, as expected (see Fig. 2e).

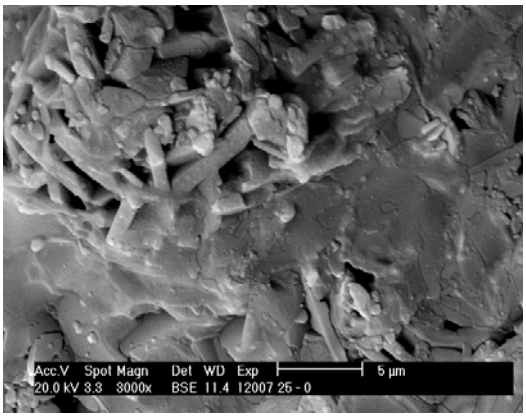

a)

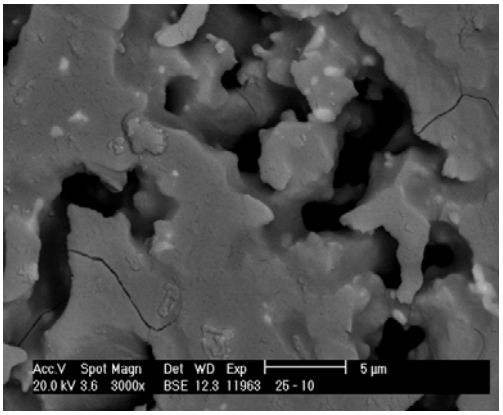

b)

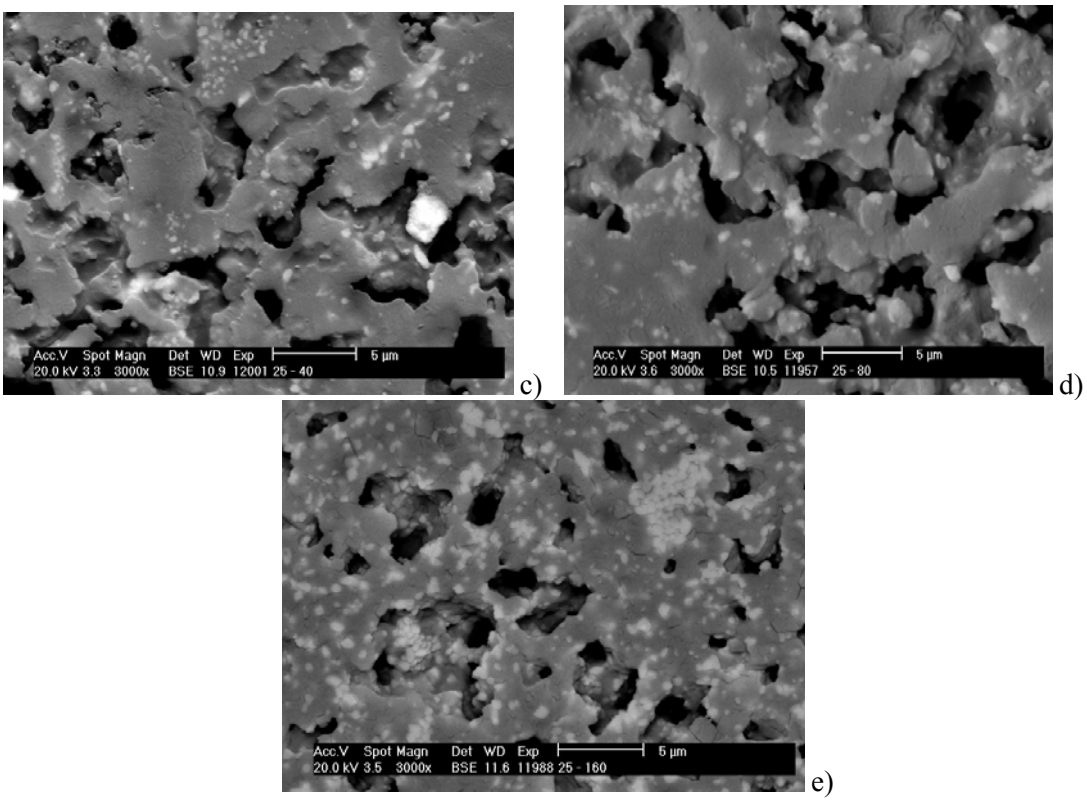

Fig. 2. Scanning electron micrographs of two-step sintered samples: a) MAS-0-S, b) MAS-10-S, c) MAS-40-S, d) MAS-80-S, and e) MAS-160-S.

The values of the obtained densities and open and closed porosity after the two-step sintering are given in Table I. The results of the sample density measurements were in agreement with the microstructural observations. The average sample densities after the two-step sintering ranged from 60.3 to 74.8 % of the theoretical densities.

Tab. I Values of density and porosity of two-step sintered samples.

Sample	Theor. dens. (gcm^{-3})	Abs. dens. (gcm^{-3})	Rel. dens. (%)	Rel. open por. (%)	Rel. clos. por. (%)
MAS-0-S	3.05	2.14	70.30	25.90	3.80
MAS-10-S	2.80	1.82	65.00	31.50	3.60
MAS-40-S	2.85	1.89	67.50	29.20	3.30
MAS-80-S	2.90	1.75	60.30	26.50	3.30
MAS-160-S	3.15	2.36	74.80	21.70	3.50

The XRD pattern of the initial non-activated sintered sample indicates that several phases – Al_2O_3, SiO_2, spinel $MgAl_2O_4$, and cordierite – are present within the MAS-0-S sintered mixture. During the sintering of the mixture activated for 10 minutes, the formation of $ZrSiO_4$ began, as a consequence of high-energy milling in the jar with ZrO_2 balls, and the presence of wet milling media. The diffraction pattern of MAS-40-S, along with well crystallized sharp peaks of cordierite and $MgAl_2O_4$, shows small amounts of Al_2O_3 and SiO_2. Except for alumina phase, the phase composition of the mixture MAS-80-S remains similar. On the contrary, the XRD pattern of the sample activated for 160 minutes and sintered indicates a cordierite phase, with $MgAl_2O_4$, zirconia compounds, without the presence of the starting phases. The increase in the milling time followed by the two-step sintering led to a better recrystallization and an increase in peak intensities, with an increased amount of the

cordierite phase, although the zirconia compounds remained.

In order to characterize the electrical properties of the sintered materials, the complex relative permittivity is measured. The starting assumption for the used procedure is that the material is linear and nonmagnetic. The complex relative permittivity is defined as $\varepsilon_r = \varepsilon_r' - j\cdot\varepsilon_r''$, where ε_r' is the real part of the complex relative permittivity, j is the imaginary unit, and ε_r'' is its imaginary part. Instead of the imaginary part, the loss tangent, defined as $\text{tg}\,\delta = \varepsilon_r''/\varepsilon_r'$, is often used. In this model, ε_r'' represents all losses in the dielectric. The real and the imaginary parts of the complex permittivity vary with frequency. The frequency variations satisfy the Hilbert transform (equivalently, they satisfy the Kramers-Kronig relations) due to the causality.

There are various options for commercially available off-the-shelf measurement systems for similar purposes, none of them has a good combination of accuracy, applicable frequency range, requirements for dimensions of the material sample, capability to measure a wide range of relative permittivities (from 1 to 1000), and an affordable market price. This has motivated us to make a custom design for the coaxial probe that can be used for the measurements in the frequency range between 1 MHz and 1 GHz.

The coaxial probe is shown in Fig. 3. It is specifically designed for measurements of the material samples of a cylindrical shape, which is one of the key requirements for sintered samples. In order to avoid the air gaps, the upper and bottom (circular) surfaces of the material sample (i.e., the cylinder) are painted with conductive liquid silver and dried for 1-2 hrs at the temperature of 120 °C. Those conductive surfaces with dielectric material between them form a parallel-plate capacitor. The upper conductive surface (i.e., the electrode) touches the inner conductor (pin) of the SMA connector that is used to feed the probe. The SMA connector has an elongated inner conductor with a dielectric around it, and the tip of the inner conductor protrudes 2.2 mm into the coaxial probe, as shown in Fig. 3b. The bottom electrode touches the base of the coaxial probe, which is a screw whose diameter is 14 mm (shown in the bottom of Fig. 3a). It can be completely unscrewed in order to put the material sample into the probe and it can be screwed into the probe to make a firm contact between conductive surfaces and the probe parts. Further, three plastic screws are used for fine adjustment of the horizontal position of the material sample in the probe (as shown in Fig. 3a). Once the position of the material sample is set, those plastic screws are taken away.

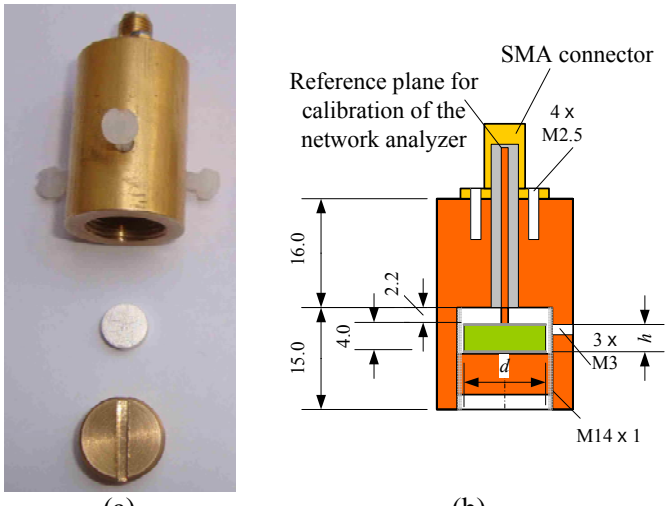

(a) (b)

Fig. 3. Custom-designed coaxial probe: a) picture and b) cross-section with designated reference plane for calibration of network analyzer. Dimensions are in millimeters.

The reflection coefficient is measured with a network analyzed connected to the probe SMA connector. We use Agilent E5061A for the measurements in the frequency range from 300 kHz to 3 GHz. The reference plane for the network analyzer calibration is shown in Fig. 3b.

For the extraction of the relative permittivity from the measured reflection coefficient, a very precise electromagnetic model of the coaxial probe and the material sample is needed. We use a quasi-static model based on the modification of the electrostatic method from [14]. The modifications include: a) improved extraction of the free-charges at the metallic surfaces so that we can analyze almost arbitrarily large relative permittivity, b) Galerkin testing within the method of moments with pulse basis functions for charge approximation, which significantly increases the accuracy of the model for a given meshing, and c) a large database of material samples with built-in interpolation so that the numerical electrostatic analysis is practically done in real-time.

In the used model, the SMA connector is very precisely modeled, as it is found that it is crucial for accurate measurements. Its electrical parameters were found to significantly deviate from nominal ones declared by the manufacturers (the measured characteristic impedance is 44 Ω as opposed to the nominal 50 Ω). Moreover, the losses in the transmission line, formed by the SMA inner conductor and the wall of the probe, are mainly due to the finite conductivity of the metallic pars. We found that the connector is made of three layers: 1) the base material is stainless (nonmagnetic) steel, 2) there is a layer of nickel on top of the steel, and 3) a thin layer of gold is deposited on top of nickel. The dominant losses at lower frequencies are in steel, at 1 GHz in nickel, and above 2 GHz in gold. Therefore, we made a three-layer analytical model for that transmission line. We have adjusted its parameters by comparison with measurements of the coaxial probe when it is empty (open) and when it is short-circuited.

Once we had the accurate model of the probe, we included the model of the material sample. It is validated by simulations that the equivalent (complex) capacitance of the material sample is a linear function of its complex permittivity. From this point onward, the measurement of the unknown complex permittivity of the material sample is straightforward. From the geometrical dimensions of the material sample and the measured capacitance (extracted the from measured reflection coefficient), the complex relative permittivity is found by interpolation in the database consisting of a large number of capacitances obtained by the electrostatic analysis.

The results for several samples are summarized in Table II. The first column in the table is the sample label, the second column is the sample diameter, the third column is the sample height, the fourth column is the capacitance of the sample extracted from the measured reflection coefficient at 100 MHz, and the last column is the estimated real part of the relative permittivity. A loss tangent was estimated to be below 0.02.

Tab. II Dimensions, capacitances, and estimated relative permittivities of samples.

Sample	Diameter (mm)	Height (mm)	Coax capacitance (pF)	Estimated ε_r'
MAS-10-S	7.84	2.98	0.904	3.622
MAS-40-S	7.71	2.81	0.903	3.622
MAS-80-S	7.83	2.77	0.912	3.460
MAS-160-S	7.14	2.59	0.975	4.746

The influence of densities on relative dielectric permittivity pointed out that the dielectric permittivity of these specimens follow the trend of density changes. Furthermore, if we compare changes in densities with activation time, clear increase of density values with prolonged milling time is noticed, owing to a lower porosity and more compact structure which is observed by changes in the microstructures. This suggests that a higher density and

the homogeneity of morphology are dominantly responsible for the higher values of dielectric permittivity of the samples. Owing to the better packaging the starting powder, of activated and hence more reactive particles, facilitated sintering, and strengthening of grain boundaries was occurred, and consequently the increase in relative density. Finally, with prolonged sintering time (from 4 to 10 h), the increase of relative permittivity for approx. 10 % was measured [10].

4. Conclusion

Based on the shown results, which present our latest work, cordierite-based ceramic materials were prepared using the two-step sintering technique. The microstructural and electrical properties of the bulk materials prepared by TSS were characterized.

The two-step sintering of the powders led to cordierite formation; prolonged second step from 4 to 10 h, is sufficient for the reaction. The densities obtained after TSS increased from 1.82 gcm^{-3} for MAS-10-S to 2.36 gcm^{-3} for MAS-160-S, respectively. The microstructures indicated porous ceramics with grains smaller than 1 μm, without grain growth with prolonged milling time. The density had the dominant influence on the dielectric permittivity (3.62 for MAS-10-S, increased to 4.75 for MAS-160-S), with a loss tangent below 0.02 for all two-step sintered samples.

Acknowledgement

This research was performed within the projects OI 172057 and TR 32005 funded by the Ministry of Education, Science and Technological Development of the Republic of Serbia, and project no. 15-06390S funded by the Grant agency of the Czech Republic. The research has been also financially supported by the Ministry of Education, Youth and Sports of the Czech Republic under the project CEITEC 2020 (LQ1601). The authors are grateful to Dr. Miodrag Mitrić, for the XRD measurements.

5. Literature

1. A.V. Ganesha, B. Basavalings, J. A. K. Tareen, M. A. Pasha, Breakdown of synthetic potassic cordierite at low P-T conditions, Curr. Sci. 87(1) (2004) 104–108.
2. Y. Kobayashi, K. Sumi, E. Kato, Preparation of dense cordierite ceramics from magnesium compounds and kaolinite without additives, Ceram.I nt. 26 (2000)739–743.
3. D. Tulyaganov, M. Tukhtaev, J. Escalante, M. J. Ribeiro, J. A. Labrincha, Processing of cordierite based ceramics from alkaline- earth aluminosilicate glass, kaolin, alumina and magnesite, J. Eur. Ceram. Soc. 22 (2002)1775–1782.
4. M. A. Camerucci, G. Urretavizcaya, A. L. Cavalieri, Sintering of cordierite based materials, Ceram. Int. 29 (2003) 159–168.
5. S. Taruta, T. Hayashi, K. Kitajima, Preparation of machinable cordierite/mica composite by low-temperature sintering, J. Eur. Ceram. Soc. 24 (2004) 3149–3154.
6. M. A. Camerucci, G. Urretavizcaya, A. L. Cavalieri, Mechanical behavior of cordierite and cordierite-mullite materials evaluated by indentation techniques, J. Eur. Ceram. Soc. 21 (2001) 1195–1204.
7. N. Moftah El-Buaishi, I. Jankovic-Castvan, B. Jokic, Dj. Veljovic, Dj. Janackovic, Rada Petrovic, Crystallization behavior and sintering of cordierite synthesized by an aqueous sol–gel route, Ceram. Inter. 38 (2012) 1835–1841.
8. N. Obradović, N. Đorđević, A. Peleš, S. Filipović, M. Mitrić, V. B. Pavlović, The

Influence of Compaction Pressure on the Density and Electrical Properties of Cordierite-based Ceramics, Sci. Sinter., 47 (2015) 15-22.
9. X.-H. Wang, X.-Y. Deng, Hai-Lin Bai, H. Zhou, Wei-Guo Qu, and L.-T. Li, Two-Step Sintering of Ceramics with Constant Grain-Size, II: $BaTiO_3$ and Ni–Cu–Zn Ferrite, J. Am. Ceram. Soc., 89 [2] (2006) 438–443.
10. N. Obradović, S. Filipović, N. Đorđević, D. Kosanović, S. Marković, V. Pavlović, D. Olćan, A. Đorđević, M. Kachlick, K. Maca, Effects of mechanical activation and two-step sintering on the structure and electrical properties of cordierite-based ceramics, Ceram. Inter., 42 (2016) 9887–9898.
11. N. Obradović, N. Đorđević, S. Filipović, N. Nikolić, D. Kosanović, M. Mitrić, S. Marković, V. Pavlović, Influence of mechanochemical activation on the sintering of cordierite ceramics in the presence of Bi_2O_3 as a functional additive, Powder Technol. 218 (2012) 157–161.
12. T. Yin, J.W. Park, S. Xiong, Physicochemical properties of nano fish bone prepared by wet media milling, LWT - Food Sci. Technol. 64 (2015) 367-373.
13. D.Y. Nhi Truong, H. Kleinke, F. Gascoin, Preparation of pure Higher Manganese Silicides through wet ball milling and reactive sintering with enhanced thermoelectric properties, Intermetall. 66 (2015) 127-132.
14. D. I. Olćan, I. M. Stevanović, J. R. Mosig, A. R. Djordjević, "Diakoptic surface integral equation formulation applied to 3-D electrostatic problems," Proc. of ACES 2007, Verona, Italy, pp. 492–498, March, 2007.

Садржај: *Керамике на бази кордијерита привлаче доста пажње због различитих примена у индустрији. Користе се за производњу вишеслојних штампаних плоча, каталитичких конвертора, филтера, топлотне изолације, пећи, компоненти преносивих електронских уређаја итд. Процес механичке активације се користи да би се смањили трошкови производње и модификовали материјали на бази кордијерита. У овом раду анализирани су микроструктура и електрична својства механички активираног система MgO-Al_2O_3-SiO_2. Смеше прахова су механички активиране у планетарном млину од 0 до 160 минута. Утицај активације и двостепеног синтеровања на микроструктуру је испитиван скенирајућом електронском микроскопијом. Електрична мерења су указала на варијације диелектричне константе (ε_r) и тангенса губитака (tg δ) у функцији времена механичког третмана.*

Кључне речи: *Механичка активација, двостепено синтеровање, микроструктура, електрична својства, кордијерит.*